2022

Development and Validation Of Resistance-Capacitance Model (RCM) For Phase Change Material (PCM) Embedded In 3D Periodic Structures

Tanjebul Alam

Giulia Righetti

Daniel Bacellar

Vikrant Aute

Simone Mancin

Development and Validation of Resistance-Capacitance Model (RCM) for Phase Change Material (PCM) Embedded in 3D Periodic Structures

Tanjebul ALAM[1], Giulia RIGHETTI[2], Daniel BACELLAR[1], Vikrant AUTE[1]*, Simone MANCIN[2]

[1]University of Maryland
College Park, MD, USA
vikrant@umd.edu

[2]University of Padova
Vicenza, Italy
simone.mancin@unipd.it

* Corresponding Author

ABSTRACT

The low thermal conductivity of Phase Change Materials (PCM) can be improved with extended surfaces such as additively manufactured 3D periodic lattice structures. Three different aluminum alloy-based lattices (base sizes 10, 20, and 40 mm) with average porosity of 0.95 filled with paraffin wax, with a nominal phase change temperature of 55°C, were experimentally investigated. In this work, a computationally efficient 2D Resistance Capacitance-based model (RCM) was developed for predicting the thermal characteristics of these geometries. Non-uniform porosity in the PCM-metal domain was estimated using image processing and served as model input. The solver does not solve for higher-order physics as in CFD but still can provide a good prediction of thermal resistance and energy storage at very low computational cost. The simulation-to-real-time factor for this geometry is of the order of 10^{-4}, while CFD simulations typically have a real-time factor greater than 1. The model was validated against the experimental data for melting under three different heat fluxes (6250 W/m^2, 12500 W/m^2 and 18750 W/m^2). The mean deviation of the predicted average PCM temperature was between 1.34 K-2.81 K for different cases. The maximum average temperature deviation of 5.45 K was observed for the 20 mm geometry at the highest heat flux test condition. The effects of natural convection were neglected in the model, but the predicted PCM temperature and energy storage still showed good agreement with the experimental data.

1. INTRODUCTION

Adding extended surfaces with high thermal conductivity can substantially increase phase change material heat exchanger (PCMHX) performance. This increase is accompanied by reduced storage potential, a trade-off that must be accounted for in the PCMHX design. There are numerous enhancement techniques such as metal fins, heat pipes, highly-conductive nanoparticles, embedding PCM in graphite or metal foams which were reviewed in detail in the following review papers by Fan & Khodadadi (2011), Elarem et al. (2020). Righetti et al. (2020a,b) investigated PCMHX's with additively manufactured aluminum structured ligaments in a lattice structure. Three different geometries with different base pore sizes were added to the PCM and the porosity was kept constant so as to compare the performance of designs with same storage potential (i.e., volume of PCM). The addition of enhancement resulted in faster energy storage and release in the PCMHX compared to a baseline design without the lattice structures. Higher number of ligaments with smaller diameter resulted in lower melting times and more uniform temperature distribution.

Researchers have developed simplified models for PCM storage devices based on resistances and capacitances (RCM). RCM does not solve for high-order physics as in CFD, however it can provide accurate prediction of heat flow and energy storage in a PCM domain with a very low computational cost. Several RCM for various applications can be found in the following works: Bontemps et al. (2011), Stupar et al. (2011), Mirzaei & Haghighat (2012) and Gao et al. (2019). These models are typically 1D and consider conduction as the dominant mode of heat transfer. Furthermore, the thermal resistance is assumed constant throughout the PCM domain. A simplified 1D RCM was developed with considering free convection during the melting process in plate storage PCMHX by Neumann et al. (2021). They used the correlations for thermal resistance estimation provided by Vogel et al. (2016); and verified the results against CFD model. The mean deviation of the fluid outlet temperature and PCM temperature between both

models was found to be 0.62 K and 0.85 K, respectively. A simulation time reduction by a factor of 20-30 compared to CFD was also reported. The geometry studied in this work required the motion of liquid PCM to be captured, but for structured designs, the natural convection effect can be less relevant, or even negligible (Alam et al., 2021a) and can be dismissed in favor of computational speed gains. A RCM for melting in composite PCM with metal foam was developed and validated against experimental data by Alam et al. (2022). The effect of natural convection was neglected here and uniform porosity in all the grids were assumed. The study compared the results against a CFD model and found negligible deviation in local temperature profile.

In this study, a computationally effective RCM is developed for the melting of PCM in different periodic structures subjected to constant heat flux. Image processing capability of a commercial software was used to find the local porosity values in the discretized grids. The model is validated against experimental data (Righetti et al., 2020b). The accuracy in prediction of average temperature profile and energy storage is discussed with the respective computational costs.

2. MODEL DESCRIPTION

2.1 Subject of Study

Figure 1 shows three different additively manufactured periodic structures which were experimentally tested under different heat flux conditions (Righetti et al., 2020b). The intersection of aluminum fibers results three pyramid structures of 40 mm, 20 mm, and 10 mm cell size. The porosity (ratio of PCM volume and container volume) for all the geometries was 0.95. Each of the geometries were filled with an organic PCM with nominal melting temperature of 55°C, and melting tests were conducted under three different heat fluxes (6250 W/m^2, 12500 W/m^2 and 18750 W/m^2). Each sample used a 20 mm thick aluminum heater block and a 12 mm thick aluminum alloy square base with an area of 1764 mm^2 for homogeneous distribution of the heat flux.

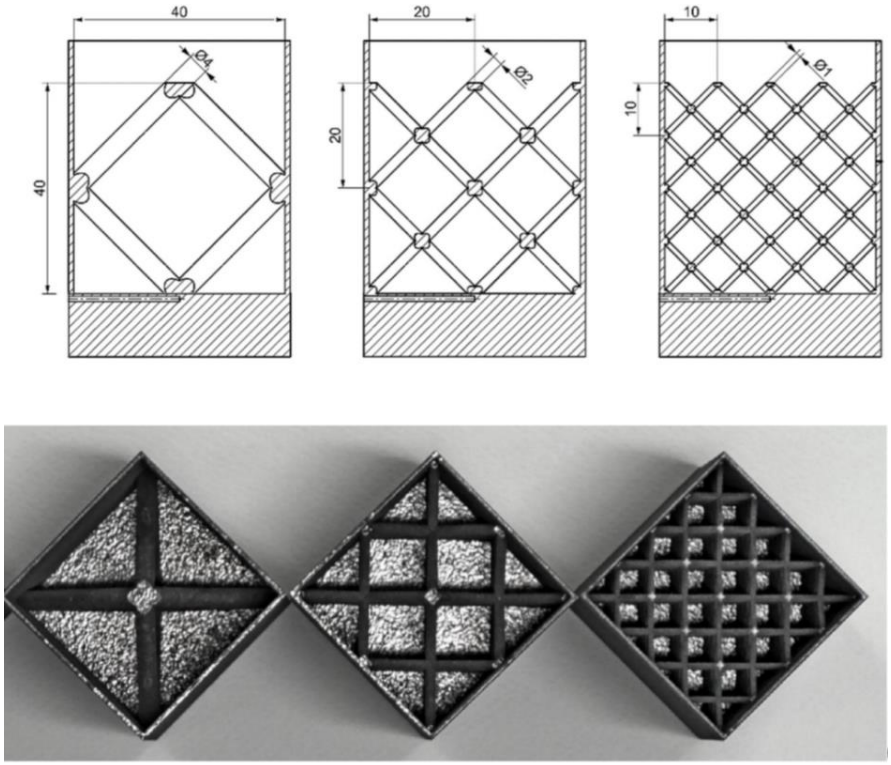

Figure 1: Additively manufactured 3D periodic structures (Righetti et al., 2020b)

AlSi10Mg-0403 aluminum alloy was used for the additive manufacturing of the periodic structures and its conductivity was measured to be 96 Wm^{-1}K^{-1} (Righetti et al., 2020b). The thermophysical properties of the PCM, aluminum, and aluminum alloy are listed in Table 1.

Table 1: Thermophysical properties

Properties	RT55	Aluminum alloy	Aluminum
k (W/m-K)	0.2	96	240
ρ (kg/m^3)	825	3745	2700
c_p (J/kg-K)	2000	1206	890
T_{sol} - T_{melt} (K)	324-330	-	-
h_s (kJ/kg)	170	-	-

2.2 Resistance Capacitance Model (RCM)

The RCM is a lightweight, computationally efficient tool that can provide good estimation of melting time and energy storage in a latent heat storage device without solving for higher-order physics. The solver takes the thermal resistances and capacitances as inputs. Figure 2 shows the thermal network of heat flow in the RCM representation of the physical models. The computational domain is discretized into segments of equal length and width, and each segment has an individual resistance and capacitance. The assumptions in the RCM model include:

- Effects of natural convection are negligible and conduction is the dominant mode of heat transfer
- No mass transfer in between segments
- PCM latent load is uniformly distributed throughout the phase-change temperature range
- The contact resistance between PCM and metal alloy is neglected

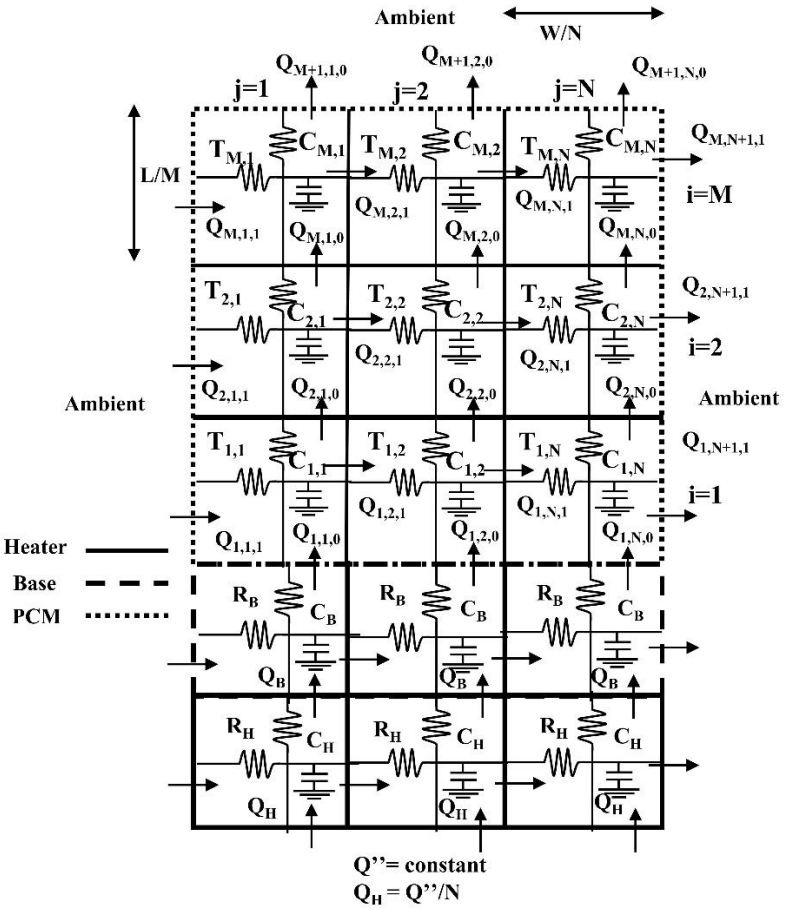

Figure 2: Thermal network of 2D RCM for periodic structures

The thermal resistance and capacitance in each of the segments are dependent upon the porosity of the segment. 2D discretization of the geometries are shown in Figure 3. In the figure, the solid black lines represent the metal structures, the dotted lines are grid lines and the white background represents the PCM. Using the image processing capability

of *MATLAB* (2018), a program is set up to read these images pixel by pixel. The number of white and black pixels in a grid provides the face area of the lattice structure in a grid and the total face area of the grid based on a 2D image. Porosity is a volume based (3D) calculation and equation *1* was used to convert the 2D area-based estimation to volume-based porosity.

$$\gamma_{i,j} = \frac{V_{PCM,i,j}}{V_{T,i,j}} = 1 - \frac{V_{alloy,i,j}}{V_{T,i,j}} = 1 - \frac{A_{alloy,i,j}}{A_{T,i,j}} \cdot \left(\frac{V_{alloy,i,j}}{V_{T,i,j}} \cdot \frac{A_{T,i,j}}{A_{alloy,i,j}}\right); \quad \frac{V_{alloy}}{V_T} \cdot \frac{A_T}{A_{alloy}} = 0.1643 \tag{1}$$

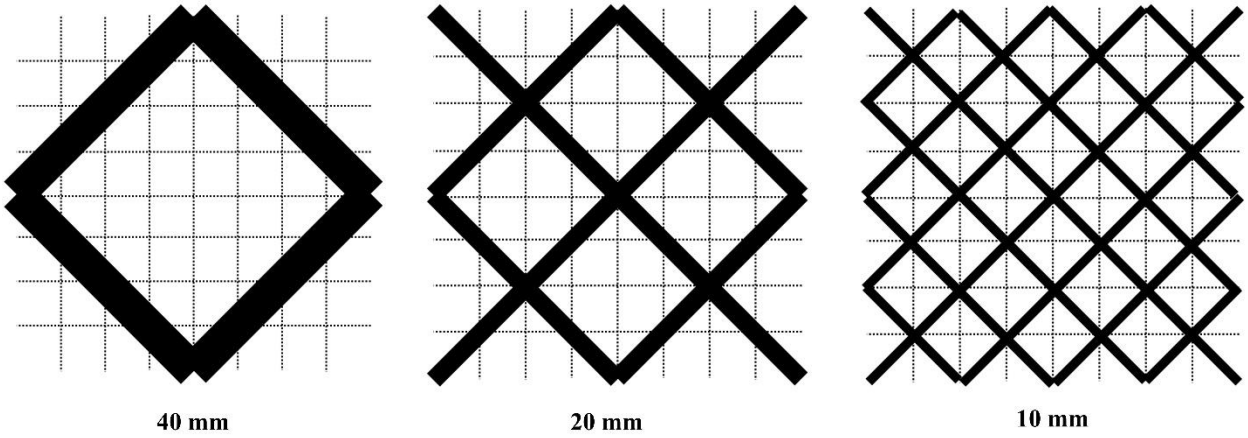

Figure 3: 2D discretization of periodic structures

The thermal network parameters then can be calculated with explicit time-marching formulation described in equations 2-13.

$$\dot{Q}_{Heater} = \dot{Q}'' \cdot A_{Base} \tag{2}$$

$$\dot{Q}_{Base,t} = \frac{T_{Heater,t} - T_{Base,t}}{R_{Heater}} \tag{3}$$

$$\dot{Q}_{i,j,t} = \frac{T_{Base,t} - T_{i,j,t}}{R_{Base}}; i = 1 \tag{4}$$

$$\dot{Q}_{i,j,0,t} = \frac{T_{i,j,t} - T_{i+1,j,t}}{R_{i,j,0}}; i \geq 2 \tag{5}$$

$$\dot{Q}_{i,j,1,t} = \frac{T_{i,j,t} - T_{i,j+1,t}}{R_{i,j,1}}; j \geq 2 \tag{6}$$

$$\frac{dT_{i,j,t}}{dt} = \frac{\dot{Q}_{i,j,0,t} + \dot{Q}_{i,j,1,t} - \dot{Q}_{i+1,j,0,t} - \dot{Q}_{i,j+1,1,t}}{C_{i,j}} \tag{7}$$

$$T_{i,j,t+\Delta t} = T_{i,j,t} + \frac{dT_{i,j,t}}{dt} \cdot \Delta t \tag{8}$$

$$R_{i,j,0} \approx R_{cond} = \frac{L/M}{k_{eff,i,j} \cdot A_{i,j}}; \tag{9}$$

$$R_{i,j,1} = \frac{W/N}{k_{eff,i,j} \cdot A_{i,j}}; R_{nat\_conv} \ll R_{cond} \tag{10}$$

$$k_{eff,i,j} = \gamma_{i,j} k_{PCM} + (1 - \gamma_{i,j}) k_{alloy} \tag{11}$$

$$C_{i,t} = [\gamma_{i,j} C_{PCM} \rho_{PCM} + (1-\gamma_{i,j}) C_{alloy} \rho_{alloy}] V_{i,j} \tag{12}$$

$$C_{PCM} = \begin{cases} c_{p,s} & \text{for } T \le T_{sol} \\ c_{p,s} + \dfrac{h_s}{T_{melt} - T_{sol}} & \text{for } T_{sol} < T < T_{melt} \\ c_{p,l} & \text{for } T \ge T_{melt} \end{cases} \tag{13}$$

Where, i denotes a specific segment lengthwise, j is widthwise (Figure 2) and t denotes a specific time step. Total volume of a segment is denoted by *V*, area of a segment is *A*, total height of the domain is *L* and width is *W*. The domain is discretized into M x N segments. $R_{i,j,t}$, $C_{i,j,t}$, $Q_{i,j,t}$, $T_{i,j,t}$ represent the thermal resistance, thermal capacitance, heat flow and temperature of a specific segment at time *t*. PCM porosity is, γ, β represents the liquid fraction, ρ, the density, and k_{eff} is the effective thermal conductivity. Figure 4 shows the solver flow chart for the RCM.

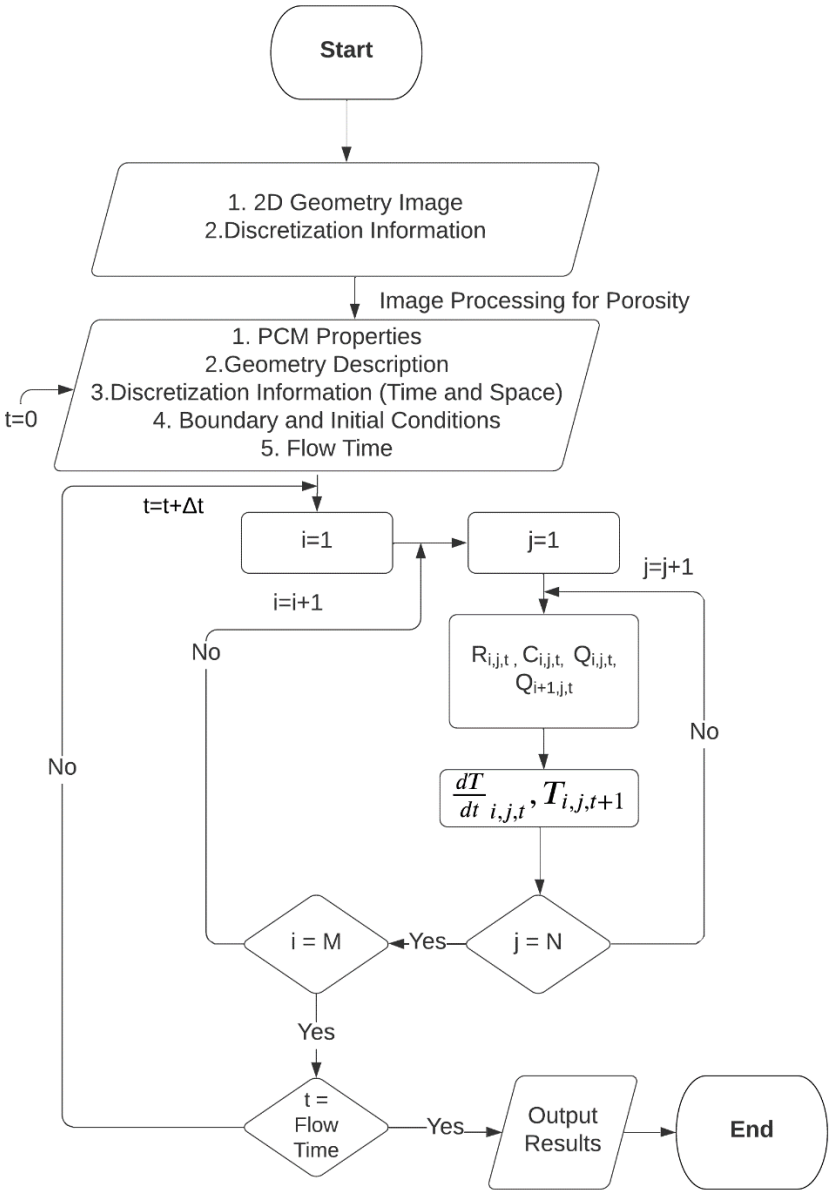

Figure 4: Solver flowchart for the RCM

Figure 5 shows the grid size and the time step independency of the RCM. In Figure 5a, RCM with 64 and 96 segments show very similar results. In Figure 5b, apart from 1s time step all the other time step selection in the RCM provided similar results. A time step size of 0.5s and grid size of 8x8 (64 segments) was selected for this work.

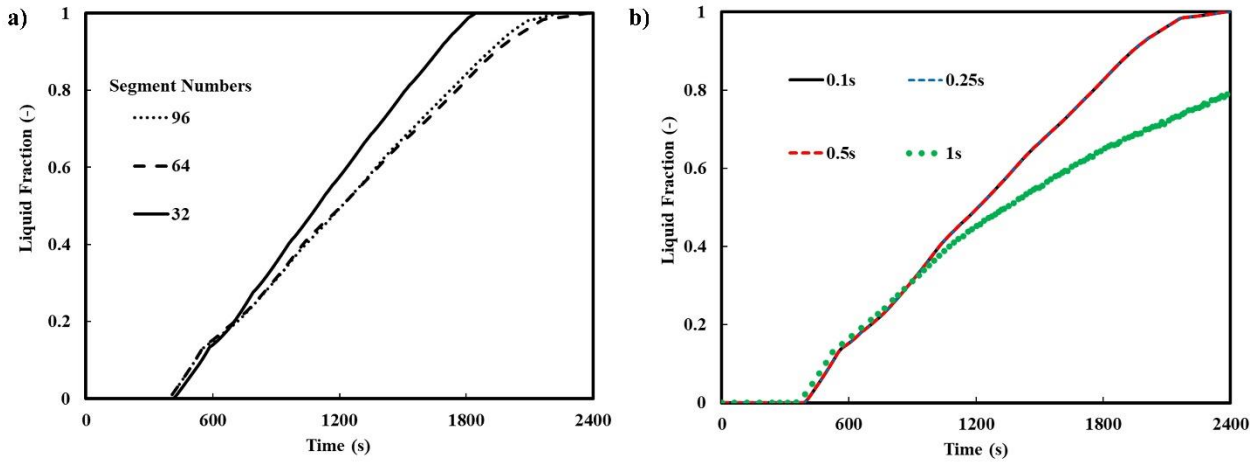

Figure 5: a) Effect of grid size, b) Effect of time step

The heat loss through the heater block was calculated using equation 14 (Righetti et al., 2020b).

$$\dot{Q}_{loss,H} = 0.0162 * T_{H,avg}\ [°C] - 0.3459\ [W] \quad (14)$$

At all side walls the heat loss were assumed to have mixed convection-radiation boundary condition. Constant heat transfer coefficient of 10 W m^{-2} K^{-1} and an emissivity of 0.95 were imposed, as suggested by Calati et al. (2021). The free stream temperature was set equal to the ambient temperature of 293 K.

3. Results

Six thermocouples were placed at different locations in the PCM domain for the experiments (Righetti et al., 2020b). The experimental PCM average temperature is found by taking the average of these temperatures. Figure 5a, 6a and 7a compare the experimental average PCM temperature profile to the RCM predicted average temperature profile for the 10 mm, 20 mm and 40 mm geometries, respectively. Each of the figures has 3 plots for three different heat flux (6250 W/m^2, 12500 W/m^2 and 18750 W/m^2) values used. The RCM predictions agree well with the experimental temperatures, in all the cases.

In RCM, the heat transfer is assumed to be conduction dominant, and the effect of natural convection is not considered. However, even though the model neglects the heat transfer enhancement by the natural convection, the results from Figures 6a, 7a, and 8a show that the average PCM temperature is slightly overpredicted by the model in most of the cases. The PCM temperature can be measured separately from the metal in the experiment and this temperature is always lower compared to the surrounding metal structures. The model assumes a single temperature for the PCM and the metal alloy and thus overpredicts the PCM temperature. The assumption to neglect the contact resistance between PCM and metal structure can also play a part in the overprediction. The heat loss calculation with a constant heat transfer coefficient may also cause some deviation in the prediction; especially at the beginning of the tests. These reasons lead to the overprediction of PCM average temperature.

Figure 6b, 7b, and 8b compare the experimental energy storage to the RCM predicted energy storage profile for the 10 mm, 20 mm, and 40 mm geometries, respectively. For both experiment and model, the energy storage at each time step is calculated using the average temperature of PCM using equations 15-16. As the storage is a direct function of the average temperature, the deviation between the model and experimental temperature causes the deviation in

storage as seen in the plots. But overall the energy storage curves show the same trend and the difference in energy storage in fully melting conditions is negligible.

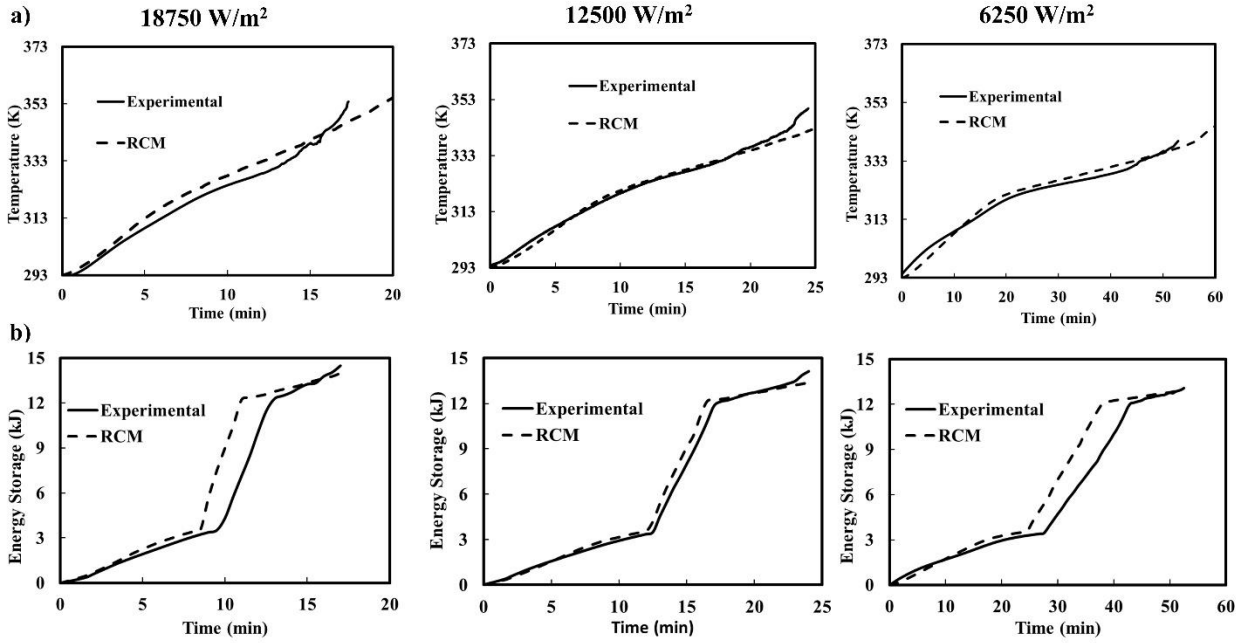

Figure 6: Comparison of experimental and RCM predicted a) Average PCM temperature b) Energy storage in 10 mm geometry

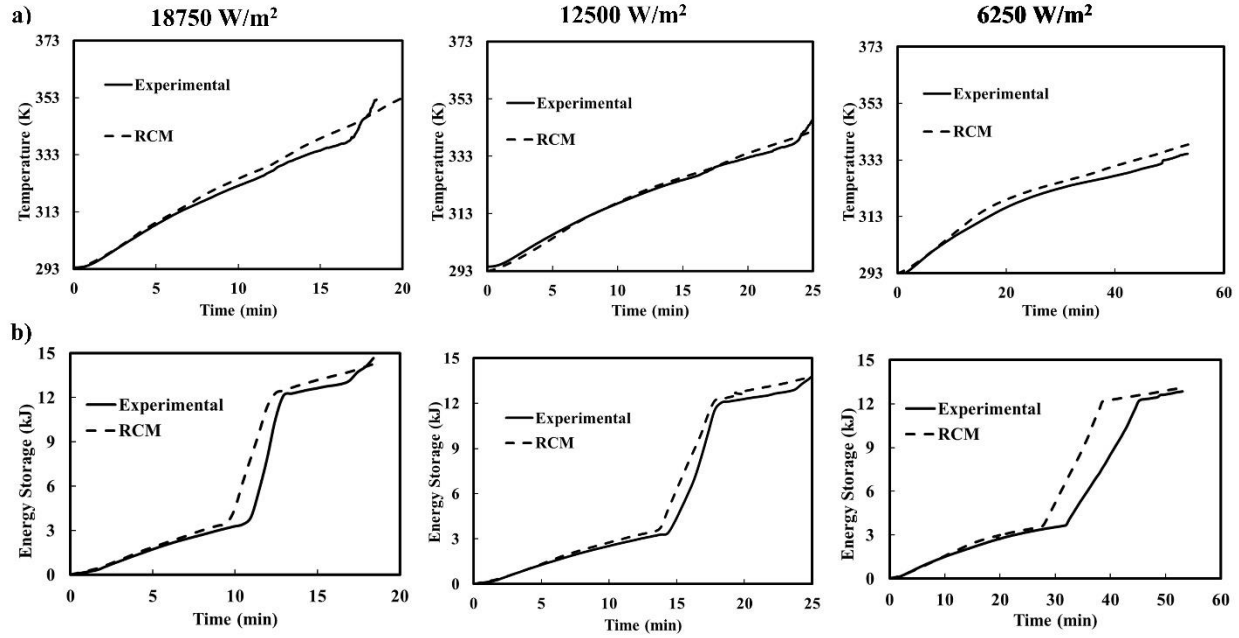

Figure 7: Comparison of experimental and RCM predicted a) Average PCM temperature b) Energy storage in 20 mm geometry

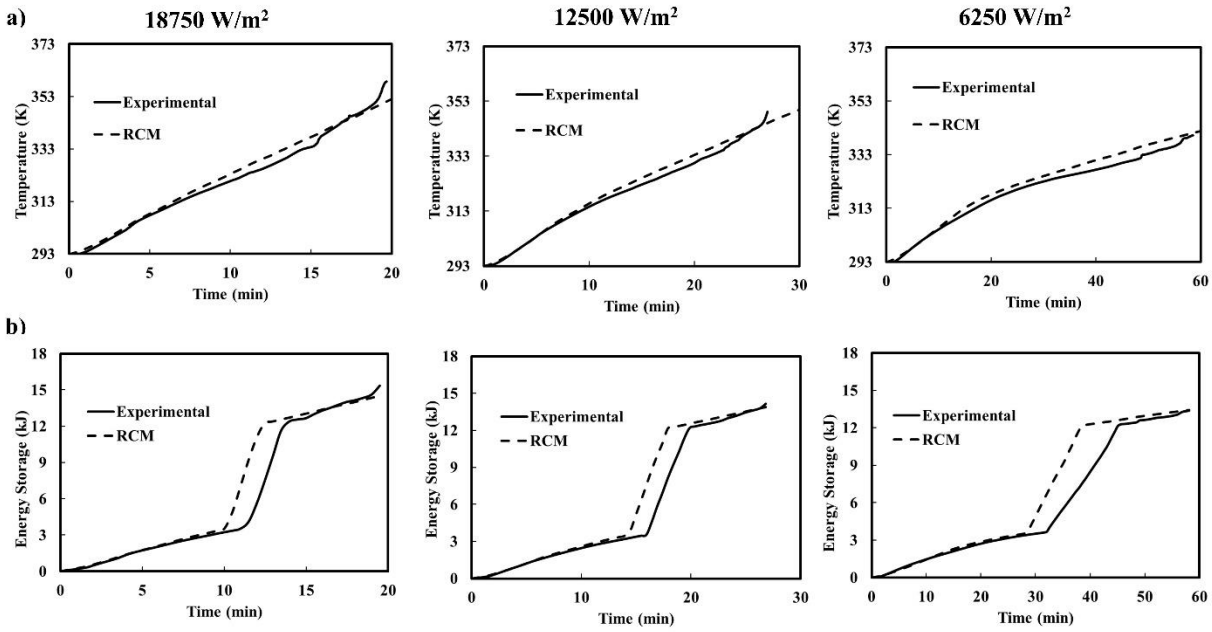

Figure 8: Comparison of experimental and RCM predicted a) Average PCM temperature b) Energy storage in 40 mm geometry

$$\beta = \frac{T_{avg} - T_{sol}}{T_{melt} - T_{sol}} \tag{15}$$

$$E_t = \begin{cases} (m_{PCM} C_{PCM} + m_{alloy} C_{alloy})(T_{avg} - T_i) & \text{for } T_{avg} \le T_{sol} \\ m_{PCM} \beta h_s + m_{alloy} C_{alloy} (T_{avg} - T_{sol}) & \text{for } T_{sol} < T_{avg} < T_{melt} \\ (m_{PCM} C_{PCM} + m_{alloy} C_{alloy})(T_{avg} - T_{melt}) & \text{for } T_{avg} \ge T_{melt} \end{cases} \tag{16}$$

3.1 Accuracy and Computational Cost

Table 2 shows the computational cost and accuracy of average temperature prediction for RCM. The table shows the mean deviation of average temperature prediction for all the cases which ranges from 1.34K to 2.81K. The table also reports the maximum deviation in average temperature found in all the cases. The maximum average temperature deviation was found to be 5.45K for the 20mm geometry for a heat flux of 18750 W/m^2. It has been observed that the PCM temperature rises abruptly at the end of melting in some of the tests. The deviation between RCM and experiment due to this sudden rise in temperature is ignored for this comparison.

Table 2: Summary of computational cost and temperature prediction accuracy

Case No	Base Diameter(mm)	Heat Flux (W/m^2)	Mean of Avg. Temperature Dev. (K)	Max. of Average Temperature Dev. (K)	Simulated Time (s)	Run Time (s)	RTF
1	10	18750	2.81	4.51	1250	0.326	2.61 x 10^{-4}
2		12500	1.34	3.30	1650	0.585	3.55 x 10^{-4}
3		6250	1.64	3.51	4200	1.305	3.11 x 10^{-4}
4	20	18750	2.15	5.45	1200	0.354	2.95 x 10^{-4}
5		12500	1.53	4.05	1800	0.602	3.34 x 10^{-4}
6		6250	2.45	3.87	3300	1.147	3.48 x 10^{-4}
7	40	18750	2.03	3.91	1500	0.444	2.96 x 10^{-4}
8		12500	1.56	3.15	1800	0.597	3.32 x 10^{-4}
9		6250	2.21	4.28	3600	1.150	3.19 x 10^{-4}

The most important aspect of the RCM is its speed and this is highlighted by the last column in the table. Here, the real-time factor (RTF) is the ratio between simulated time and simulation time required for the model. In all the cases, the RCM RTF was found to be in the order of 10^{-4}, whereas, in CFD the RTF is a value typically much greater than 1 (Alam et al., 2021b). The results from Table 2 shows that RCM has very low computational cost with minimal penalty in accuracy.

4. CONCLUSIONS

A lightweight resistance-capacitance model (RCM) was developed for the melting of PCM in periodic lattice structures with constant heat flux. The model neglects the effect of natural convection and takes the non-uniform distribution of the metal into account by estimating area-based porosity and converting it to volume-based porosity. The model was validated against experimental data and shows good prediction of both average PCM temperature and energy storage. The simulation real-time factor of the model is of the order of 10^{-4} and the accuracy penalty is negligible compared to the speed of the model.

NOMENCLATURE

A	Area	(m^2)
c_p	Specific heat	(J/kg-K)
C	Heat capacity	(J/kg-K)
E	Energy storage	(J)
h_s	Latent heat	(J/kg)
k	Thermal conductivity	(W/m-K)
L	PCM domain length	(m)
m	Mass	(kg)
M	Number of segments lengthwise	(-)
N	Number of segments widthwise	(-)
$\dot{Q}$	Heat flow	(W)
$\dot{Q}$”	Heater heat flux	(W/m^2)
$\dot{Q}_{loss,H}$	Heater heat loss	(W)
$T_{H,avg}$	Heater average temperature	(°C)
T_{sol}	Solidification temperature	(K)
T_{melt}	Liquidous temperature	(K)
T	Temperature	(K)
Δt	time step size	(s)
R	Thermal resistance	(K/W)
RTF	Real-time factor	(-)
V	Volume	(m^3)
W	PCM domain width	(m)
β	Liquid fraction	(-)
γ	Porosity	(-)
ρ	Density	(kg/m^3)

Subscripts

eff	Effective
i	Specific segment number (lengthwise)
j	Specific segment number (widthwise)
t	Specific timestep
s	Solid phase
l	Liquid phase
0	lengthwise direction
1	widthwise direction

REFERENCES

Alam, T., Bacellar, D., Ling, J., & Aute, V. (2021a). Effect of thermal expansion coefficient, viscosity and melting range in simulation of pcm embedded heat exchangers with and without fins. *International Mechanical Engineering Congress and Exposition*.

Alam, T., Bacellar, D., Ling, J., & Aute, V. (2022). Development and Validation of Resistance- Capacitance Model for Phase Change Material Embedded in Porous Media. 2022 21st *IEEE Intersociety Conference on Thermal and Thermomechanical Phenomena in Electronic Systems (ITherm)*.

Alam, T., Bacellar, D., Ling, J., & Aute, V. (2021b). Numerical Study and Validation of Melting and Solidification in PCM Embedded Heat Exchangers with Straight Tube. *18th International Refrigeration and Air Conditioning Conference at Purdue*, 1–8.

Bontemps, A., Ahmad, M., Johanns, K., & Sallée, H. (2011). Experimental and modelling study of twin cells with latent heat storage walls. *Energy and Buildings*, *43*(9), 2456–2461. https://doi.org/10.1016/j.enbuild.2011.05.030

Calati, M., Guarda, D., Righetti, G., & Zilio, C. (2021). Numerical Modelling of a PCM Embedded in Periodic Structures. *13th IIR Conference on Phase-Change Materials and Slurries for Refrigeration and Air Conditioning*. https://doi.org/10.18462/iir.PCM.2021.2203

Elarem, R., Alqahtani, T., Mellouli, S., Askri, F., Edacherian, A., Vineet, T., Badruddin, I. A., & Abdelmajid, J. (2020). A comprehensive review of heat transfer intensification methods for latent heat storage units. *Energy Storage*, *December*, 1–30. https://doi.org/10.1002/est2.127

Fan, L., & Khodadadi, J. M. (2011). Thermal conductivity enhancement of phase change materials for thermal energy storage: A review. *Renewable and Sustainable Energy Reviews*, *15*(1), 24–46. https://doi.org/10.1016/j.rser.2010.08.007

Gao, J., Yan, T., Xu, T., Ling, Z., Wei, G., & Xu, X. (2019). Development and experiment validation of variable-resistance-variable-capacitance dynamic simplified thermal models for shape-stabilized phase change material slab. *Applied Thermal Engineering*, *146*(July 2018), 364–375. https://doi.org/10.1016/j.applthermaleng.2018.09.124

MATLAB (9.6.0.1072779 (R2019a)). (2018). The MathWorks Inc.

Mirzaei, P. A., & Haghighat, F. (2012). Modeling of phase change materials for applications in whole building simulation. *Renewable and Sustainable Energy Reviews*, *16*(7), 5355–5362. https://doi.org/10.1016/j.rser.2012.04.053

Neumann, H., Gamisch, S., & Gschwander, S. (2021). Comparison of RC-model and FEM-model for a PCM-plate storage including free convection. *Applied Thermal Engineering*, *196*(September 2020), 117232. https://doi.org/10.1016/j.applthermaleng.2021.117232

Righetti, G., Savio, G., Meneghello, R., Doretti, L., & Mancin, S. (2020). Experimental study of phase change material (PCM) embedded in 3D periodic structures realized via additive manufacturing. *International Journal of Thermal Sciences*, *153*(October 2019), 106376. https://doi.org/10.1016/j.ijthermalsci.2020.106376

Stupar, A., Drofenik, U., & Kolar, J. W. (2011). Application of phase change materials for low duty cycle high peak load power supplies. *2010 6th International Conference on Integrated Power Electronics Systems, CIPS 2010*, 16–18.

Vogel, J., Felbinger, J., & Johnson, M. (2016). Natural convection in high temperature flat plate latent heat thermal energy storage systems. *Applied Energy*, *184*, 184–196. https://doi.org/10.1016/j.apenergy.2016.10.001

ACKNOWLEDGEMENT

This material is based upon work supported by the U.S. Department of Energy's Office of Energy Efficiency and Renewable Energy (EERE) under the Building Technologies Office Award Number DE-EE0009158. The views expressed herein do not necessarily represent the views of the U.S. Department of Energy or the United States Government. This work was also funded in part by the Modeling and Optimization Consortium at the University of Maryland.